RESEARCH ARTICLE

Macromolecular Chemistry and Physics

www.mcp-journal.de

Smart Microgels from Unconventional Acrylamides

*Yvonne Hannappel, Lars Wiehemeier, Maxim Dirksen, Tilman Kottke, and Thomas Hellweg**

In the present study, smart responsive microgels are synthesized from a series of alternative monomers, which are less common in micro- and nanogel research. Their swelling behavior is studied by means of photon correlation spectroscopy and Fourier transform infrared spectroscopy. In addition, these monomers are used to make copolymer microgels. In line with previous results for such copolymer particles the present work observes linear changes of the volume phase transition temperatures of the microgels as a function of the microgel composition. The presented systems allow to realize a broad range of transition temperatures, which is potentially interesting for applications in sensing, actuation, and drug delivery.

1. Introduction

Since nearly 40 years so-called smart microgels have been studied due to their unique response to changes of temperature, pH, or ionic strength.[1] Most studies focused on the temperature dependent reversible swelling and de-swelling of these colloidal gel networks and their fascinating properties were already subject of several reviews.[2–11] Smart microgels are interesting model systems for colloid physics.[12–14] Recently, so-called ultra low cross-linked microgels[14,15] and hollow microgels[16,17] came into focus in this area. Hollow microgels are obtained by hydrolysis of the silica cores in core–shell microgels.[18] These two systems are interesting with respect to applications but also with respect to the answer of fundamental questions about the interaction of ultra-soft particles and about the transition from particle like behavior to polymer like behavior.[19,20]

Moreover, microgels are also very promising for several applications for example, in cell culture of vertebrate cells,[21,22] in sensor development,[23,24] for drug delivery,[25–28] hyperthermia,[29] or in catalysis.[30,31]

Dr. Y. Hannappel, Dr. L. Wiehemeier, M. Dirksen, Prof. T. Kottke, Prof. T. Hellweg
Physical and Biophysical Chemistry
Bielefeld University
Universitätsstr. 25, 33615 Bielefeld, Germany
E-mail: thomas.hellweg@uni-bielefeld.de

The ORCID identification number(s) for the author(s) of this article can be found under https://doi.org/10.1002/macp.202100067

DOI: 10.1002/macp.202100067

The best studied polymer in the context of microgels is poly(*N*-isopropyl acrylamide) (PNiPAM) cross-linked with *N,N'*-methylene bisacrylamide (BIS).[1] However, many other acrylamide derivatives also lead to polymers and gels with responsive properties for example, polyvinylcaprolactam[32,33] or poly(*N*-isopropyl methacrylamide) (PNiPMAM).[26,34,35] Such systems are less studied compared to PNiPAM. This might be due to the fact that often it is wrongly assumed that these polymers behave exactly like PNiPAM and no new properties arise from such alternative monomers. Nevertheless, in a recent work it was shown that poly(*N*-*n*-propylacrylamide) (PNnPAM) microgels exhibit important differences compared to PNiPAM.[36,37] The volume phase transition (VPT) of such PNnPAM particles is significantly sharper compared to PNiPAM microgels and the transition is found to occur within a temperature range of ≈0.1 K.[36] Moreover, alternative monomers are also interesting when copolymerized with NiPAM for example, allowing to continuously tune the volume phase transition temperature (VPTT) of the obtained particles[38] or to obtain pH sensitive microgels upon incorporation of acrylic acid,[39,40] methacrylic acid,[28,41–43] or vinylacetic acid.[44] Hence, despite of the broad body of literature on PNiPAM based microgels it is still relevant to synthesize and study systems based on alternative monomers.

There are several acrylamide and methacrylamide monomers which are known to form thermo-responsive water soluble linear homo-polymers. To synthesize these monomers, for example with different substituents at the nitrogen atom or the double bond, mainly the reaction of acryloyl chloride or methacryloyl chloride and an amine is performed in a dichloromethane/sodium carbonate solution[45–47] or in benzene.[48,49] In our group the Schotten–Baumann type reaction published by Hirano et al. for NnPAM[45] is well-established and the desired monomer can be obtained with high quality and good yield.[37,50] Based on this approach, in the present work we present the synthesis of alternative polymerizable acrylamides and methacrylamides by the reaction of acryloyl chlorides and primary or secondary amines. Moreover, these monomers are subsequently polymerized in a standard precipitation polymerization in presence of a cross-linker and the size, polydispersity, and swelling behavior of the obtained microgel particles are investigated by atomic force microscopy (AFM), attenuated total reflection Fourier transform infrared spectroscopy (ATR-FTIR), and photon correlation spectroscopy (PCS). In addition the respective copolymer microgels with NiPAM or NiPMAM for all

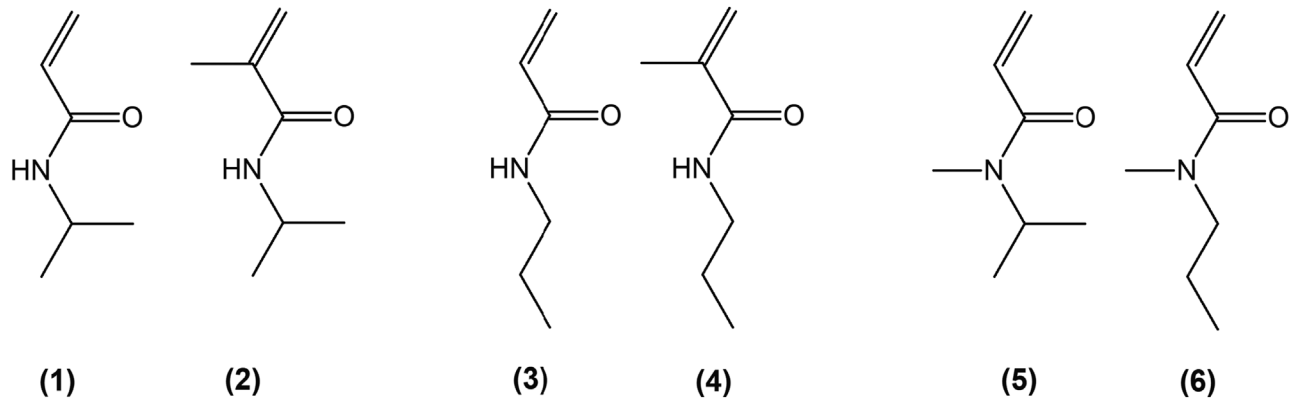

Figure 1. Structural formulas of different (meth)acrylamides for the synthesis of thermo-responsive microgels via precipitation polymerization: NiPAM (1) , NiPMAM (2), NnPAM (3), NnPMAM (4), NiPNMeAM (5), and NnPNMeAM (6).

other synthesized monomers are made and characterized. In line with previous work, also for these copolymer microgel particles a linear relationship between the VPTT and the comonomer ratio is found.

2. Results and Discussion

2.1. Alternative Monomers

We have synthesized several alternative monomers which are known or expected to lead to polymers with a lower critical solution temperature (LCST). All monomers were made following the work by Hirano and co-workers[45] (for the detailed synthesis and characterization see Supporting Information). Subsequently, we aimed at synthesizing alternative microgels with a thermo-responsive behavior and unfamiliar VPTTs via a standard precipitation polymerization. In **Figure 1** the already widely used and commercially available monomers NiPAM and NiPMAM, as well as the rarely used acrylamides, NnPAM and *N*-*n*-propylmethacrylamide (NnPMAM) and the not yet exploited monomers *N*-isopropyl-*N*-methylacrylamide (NiPNMeAM), *N*-*n*-propyl-*N*-methylacrylamide (NnPNMeAM) are presented.

An often used procedure to investigate the LCST behavior of non-NiPAM based acrylamide polymers in water is to synthesize linear polymers in organic solvent using a free radical polymerization.

N-*n*-propylmethacrylamide is the homologous monomer to NnPAM just with an additional methyl group at the double bond. There are only a few studies on the synthesis and polymerization of NnPMAM[46,49,51–53] and no microgel particles, at least to our knowledge, have been prepared from this monomer yet. In most cases a free radical polymerization using methanol as solvent and α,α'-azobis(isobutyronitrile) as initiator was performed and yielded linear polymers with different mean molecular weights. For example, Maeda et al. synthesized linear polymers of NnPMAM and NiPMAM in methanol and characterized the phase transition in water and D_2O by using FTIR spectroscopy.[48] This work reports that the methyl-substituted polymer showed a larger thermal hysteresis of the phase transition than the homologous PNiPAM and PNnPAM and verified differences in hydrogen bonding at the amide C=O groups. The phase transition temperature varied in a large range depending on the sample concentration, the solvent and the heating/cooling process.

The linear polymers showed a thermoresponsive behavior with a more or less pronounced hysteresis between the heating and cooling cycle.[51,52] Moreover, the binodal lines of the binary systems polymer/water were found to depend significantly on the sample concentration and phase separation occurs between 32[49,51–53] and 36 °C as a function of polymer concentration.[46,52]

2.2. Homopolymer Microgels

Thermo-responsive microgel particles based on the monomer NiPAM and NiPMAM are well known and widely used. Furthermore, microgels made of NnPAM are described by Kano et al.,[49] Matsumara et al.,[54] Uchiyama et al.,[55] and since 2012 by our group in several publications.[37,38,56–60] But to our knowledge, the preparation and characterization of microgels based on the other monomers mentioned above (see Figures 1 and 4–6) has only been described once for NnPMAM by our group.[37]

Accordingly, homopolymer microgel particles of all six acrylamides were synthesized under identical conditions, that is equal amounts of cross-linker, surfactant (SDS), and initiator, constant reaction volume of 10 mL and identical polymerization temperature and duration. A characterization of the resulting microgel particles was performed by PCS and AFM and the results are summarized in the following sections.

2.2.1. PCS on Homopolymer Microgels

PCS allows us to obtain the time intensity correlation functions of the light scattered from the microgel solutions. These are subsequently analyzed leading to the determination of the relaxation rate Γ. The intensity time correlation functions were converted to the respective field time correlation functions and analyzed by Laplace inversion. For all angle-dependent measurements three correlation functions per scattering angle were recorded at different angles between 30° and 120 ° and for two temperatures T. The computed relaxation rate Γ, was averaged and plotted versus the square of the magnitude of the scattering vector q^2. **Figure 2**

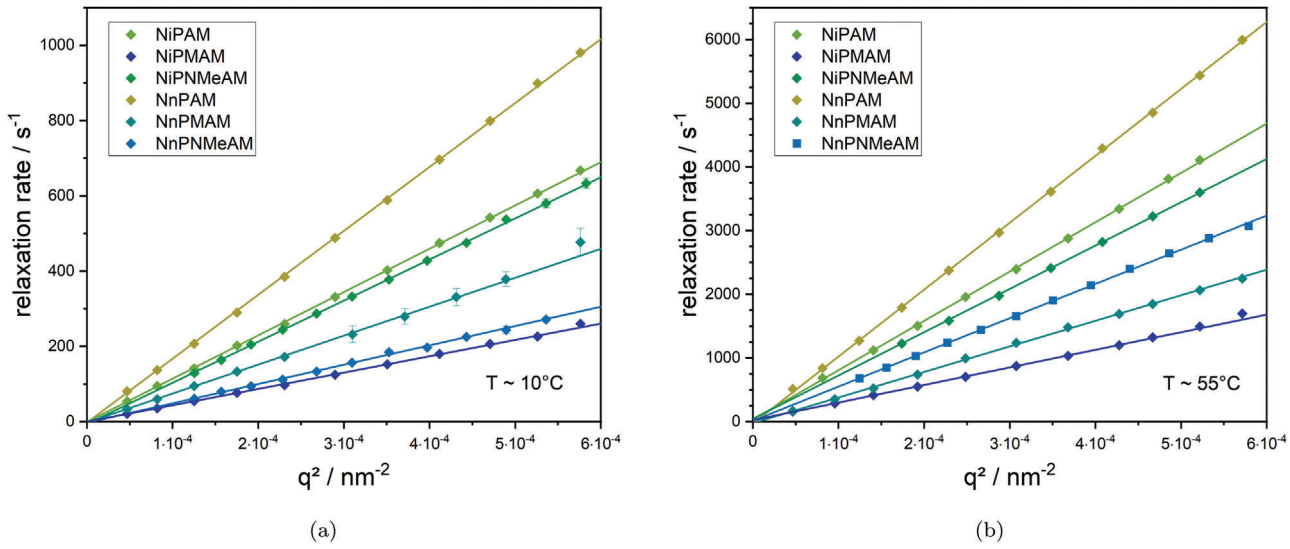

Figure 2. Averaged relaxation rates $\bar{\Gamma}$ for the different synthesized homopolymer microgels at two temperatures a) $T = 10\,°C$: swollen state; b) $T = 55\,°C$: collapsed state. The respective correlation functions were measured three times each at 11 different scattering angles. For all particles the data follow the expected linear behavior indicating purely diffusional dynamics. Within the experimental precision all fits go through the origin (see Equation (1)).

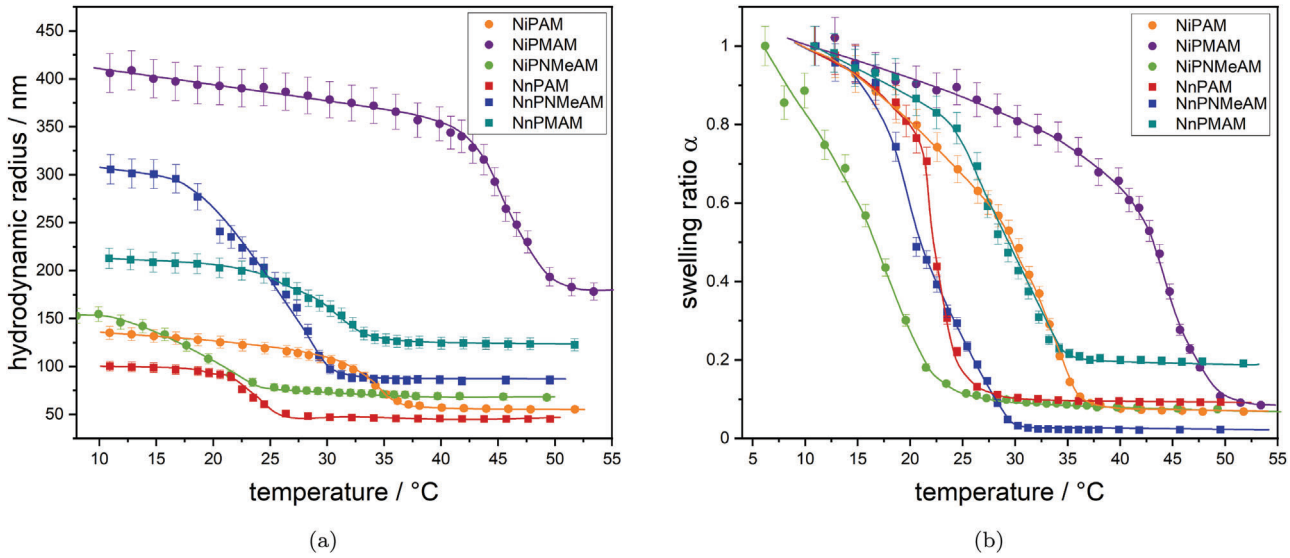

Figure 3. Temperature induced phase transition represented by the change in a) hydrodynamic radius for different acrylamide homopolymers (the lines are only guides) and b) swelling ratio.

displays the obtained mean relaxation rates $\bar{\Gamma}$ for the different homopolymer microgels. All samples show purely diffusional dynamics within the experimental precision. From a linear fit, the translational diffusion coefficient D^T

$$\bar{\Gamma} = D^T q^2 \tag{1}$$

is obtained. D^T was used to further calculate the respective hydrodynamic radius $R_h = k_B T/(6\pi\eta D^T)$. Here, k_B is the Boltzmann constant and η is the solvent viscosity. In addition, the analysis of the correlation functions also gives access to the relative size polydispersity of the microgels which is found to be between 4% and 8% (see Table S1, Supporting Information). These low values are typical for precipitation polymerization.

Figure 3 reflects the volume phase transition of the homopolymer microgel particles in terms of the decrease in hydrodynamic radius as a function of temperature. At temperatures above the LCST of the polymer the solubility of the acrylamide network decreases. As a consequence the network collapses and the particle size is reduced. Due to the fact that all synthesized particles are very different in size below and above the VPTT, the swelling ratio α was additionally calculated (see Equation (2)) and plotted as a function of the temperature. Since we are dealing with microgels of nearly spherical shape in solution, the radius can be used to calculate α.

$$\alpha = \frac{V_{collapsed}}{V_{swollen}} = \left(\frac{R_h(T)}{R_0}\right)^3 \tag{2}$$

Table 1. VPTTs of the homopolymers obtained from the PCS swelling curves.

	NiPAM	NiPMAM	NiPNMeAM	NnPAM	NnPMAM	NnPNMeAM
$VPTT_{PCS}$	34.2 °C	45.3 °C	18.7 °C	22.8 °C	29.3 °C	26.6 °C

$R_h(T)$ is the hydrodynamic radius at a certain temperature and R_0 is the hydrodynamic radius in the fully swollen state. In this work for R_0 the hydrodynamic radius at a temperature of ≈10 °C is used. The trend of the commonly used homopolymers (PNiPAM, PNiPMAM, and PNnPAM) is well comparable with data from literature[50]: here, PNnPAM shows a sharp phase transition whereas PNiPAM and PNiPMAM exhibit a broader, continuous phase transition. For PNnPMAM the way the swelling curve decays with temperature is comparable to findings by Wrede et al.[37] Looking at the particle size it is noticeable that the introduction of a methyl group at the double bond of the acrylamide monomers NiPAM and NnPAM (→ NiPMAM and NnPMAM) results in both cases in an increase in particle size. This might indicate that during the nucleation phase of the precipitation polymerization a smaller amount of precursor particles is formed, maybe caused by a generally slower polymerization of methacrylamides (forming a more stable radical), and these precursors finally yield less but larger microgel particles. If a methyl group is present at the nitrogen atom of the acrylamide monomers NiPAM and NnPAM (→ NiPNMeAM and NnPNMeAM) no common trend regarding the particle size is recognizable. However, a broadening of the phase transition is observed.

The first derivative of the swelling curves in Figure 3a and their point of inflection is used to determine the VPTT. The values calculated this way are summarized in **Table 1** and are for the well characterized polymers (PNiPAM, PNiPMAM, PNnPAM, and PNnPMAM) in good agreement with values from literature for similar homopolymer microgels.[37,50] The introduction of a methyl group at the double bond shifts the VPTT of the polymer to higher temperatures which is consistent with the fact that poly(alkylmethacrylamide) derivatives generally exhibit a higher LCST than poly(alkylacrylamide) polymers with identical side chain.[51,61,62] In the case of NiPNMeAM and NnPNMeAM there is no indication of a systematic increase/decrease of the VPTT with the introduction of a methyl group at the N-atom.

2.2.2. AFM of Homopolymer Microgels

Figure 4 shows AFM phase images of the three homopolymer microgels made of the alternative monomers. Based on these experiments, the NnPMAM homopolymer microgel seems to have the most compact and rigid structure. Almost no phase difference can be seen in the AFM phase image. Since the initial amount of BIS was equal for all homopolymers, it is likely that the incorporation of the cross-linker in NnPMAM is homogeneous.

If the phase image of PNiPNMeAM is considered, a clear phase difference between the particle interior and the observable corona can be recognized. The presence of this core–shell structure is maybe caused by a faster polymerization of BIS at the beginning of the microgel particle formation, which results in a more cross-linked core and a less cross-linked shell. This would mean that an additional methyl group at the nitrogen atom of the monomer significantly changes the copolymerization parameters of the monomer and cross-linker. To ensure that the formation of the core–shell structure is not caused by the AFM sample preparation on PEI coated wafers, PNiPNMEAM was also investigated on uncoated wafers. In these AFM images (see Figure S1, Supporting Information) a core–shell structure is also visible, confirming the previous assumption.

This trend continues with PNnPNMeAM homopolymer microgels. First of all, the phase pattern of these particles differs from the previously considered homopolymers. More domains with a slight phase difference can be observed. The domains indicate an inhomogeneous incorporation of the cross-linker. From the corresponding AFM height images (Figure S2, Supporting Information) height profiles for the three homopolymers were extracted and are summarized in Figure 4d. It is obvious that the PNnPMAM microgels deform less in height during the drying process on the wafer and thus exhibit a more rigid structure than PNiPNMeAM and PNnPNMeAM. These observations are in a good agreement with the swelling ratios of the microgels obtained by the PCS measurements (Figure 3b). Here the PNnPMAM particles show a less pronounced swelling behavior in line with a tighter network compared to the N-methylated homopolymers.

Since the initial feed of *N,N'*-methylene bisacrylamide (BIS) was equal for all homopolymers, a different degree of cross-linking can also be explained by a lower total incorporation of BIS during the microgel synthesis for the N-methylated homopolymers. However, this is rather unlikely. The height profiles also allow a determination of the particle dimensions in lateral direction. It should be noted that due to interactions of the microgels with the silicon wafer and due to drying effects, the size of the particles observed by AFM differs from the size of the collapsed particles in solution determined by PCS. However, the trend observed by AFM is the same as in the PCS study: PNnPMAM leads to the largest particles. Microgels based on PNiPNMeAM and PNnPNMeAM are significantly smaller. Further, PNiPNMeAM and PNnPNMeAM homopolymer particles show a greater lateral expansion on the substrate compared to PNnPMAM particles.

AFM pictures of PNiPAM, PNiPMAM, and PNnPAM microgels for comparison can be found in Wedel et al.[50]

2.3. Copolymer Microgels

In earlier work about copolymer microgels of NnPAM and NiPMAM, we have already shown that a linear relation exists between the VPTT and the monomer composition in the copolymer microgel.[38] To check if this also holds for other acrylamide monomers we synthesized a variety of different copolymer particles containing the monomers NnPMAM, NiPNMeAM, and NnPNMeAM in combination with NiPAM and NiPMAM, respectively.

2.3.1. FTIR Spectroscopy: Copolymer Composition

Inspired by the versatile microgel copolymer systems based on NiPAM, NiPMAM, and NnPAM, we first synthesized a series

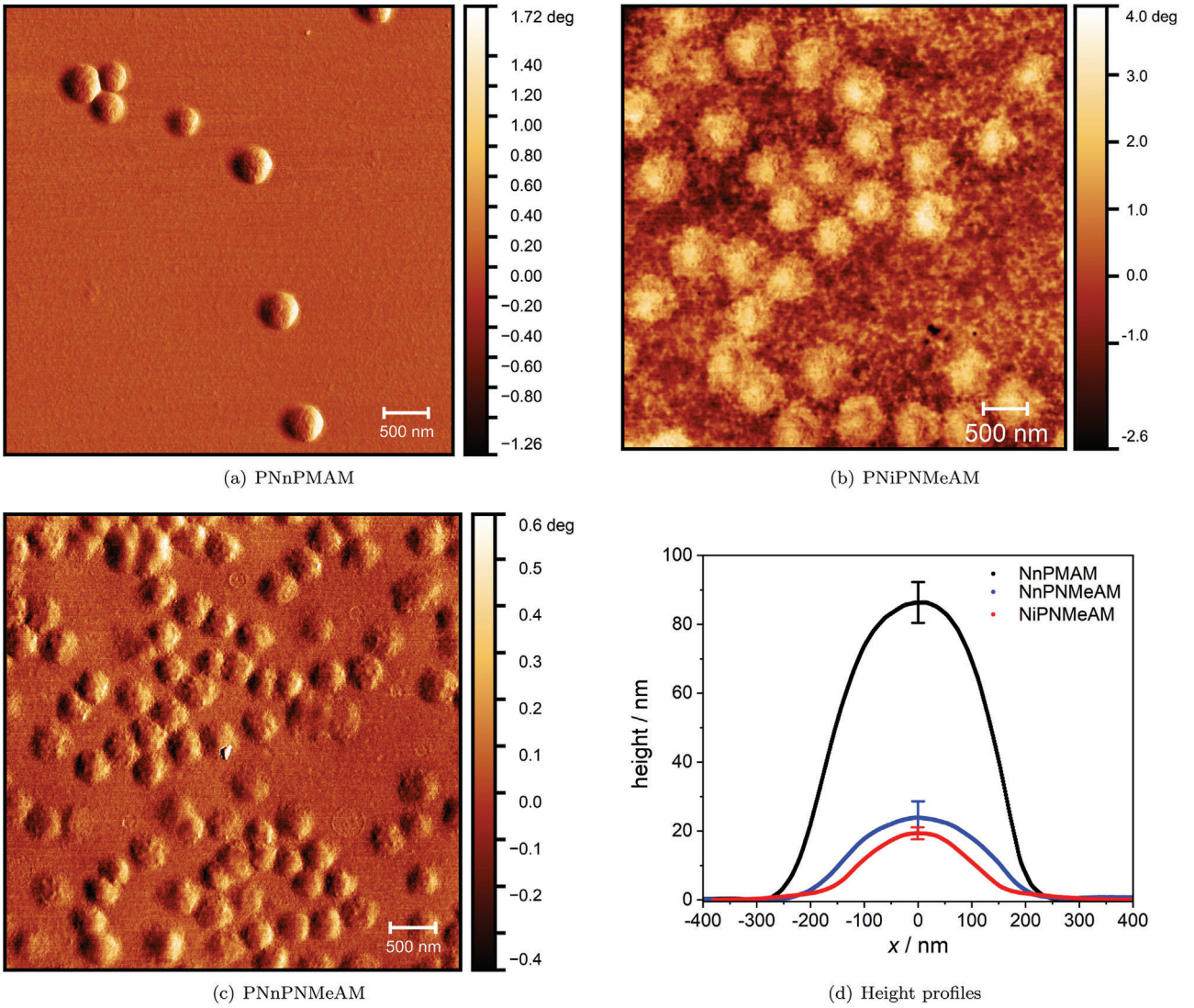

Figure 4. AFM phase images of homopolymer microgel particles made of a) NnPMAM, b) NiPNMeAM, and c) NnPNMeAM. All measurements were performed in the dry state at room temperature. The corresponding height images are shown in the Supporting Information. In (d) the respective typical height profiles of the three homopolymer microgels are shown.

of statistical copolymer microgels of NnPMAM in combination with NiPAM and characterized the particle properties and phase transition behavior. Since the transition temperatures of PNiPAM and PNnPMAM are similar, a NnPMAM/NiPMAM copolymer microgel system was additionally synthesized. Furthermore, also NiPNMeAM and NnPNMeAM are combined with NiPAM to obtain statistical copolymer microgels.

The actual monomer composition in the copolymer microgels was identified by ATR-FTIR spectroscopy. For this purpose a small volume of microgel suspension was dried on the ATR crystal and spectra of all copolymers were recorded. To determine the degree of copolymerization in the copolymer microgels, the normalized spectra were fitted with a linear combination of the spectra of the respective homopolymer particles. As an example **Figure 5**a shows the normalized FTIR spectra and the corresponding fit based on a linear combination of the respective homopolymer spectra. From the obtained coefficients of the linear combination, the degree of copolymerization was calculated. A summary of the calculated copolymer compositions is given in Figure 5b depending on the monomer feed in the synthesis.

The results of the FTIR measurements prove a successful copolymerization of the different monomers. However, they also show that the alternative monomers are incorporated with varying success with respect to the initial feeds used in the synthesis.

For the monomers with an additional methyl group at the nitrogen atom (NiPNMeAM (red ▲) and NnPNMeAM (black ◆) in Figure 5b) an approximately linear relation between monomer feed and actual incorporation is observed. Deviations from the ideal behavior indicated by the dashed black line are small. A more interesting behavior is observed for the microgels synthesized with NnPMAM as second monomer: the copolymer particles based on P(NiPAM-*co*-NnPMAM) (Figure 5b blue •) contain a decreased amount of NnPMAM compared to the initial feed. However, if NiPAM is replaced by NiPMAM, the polymerization

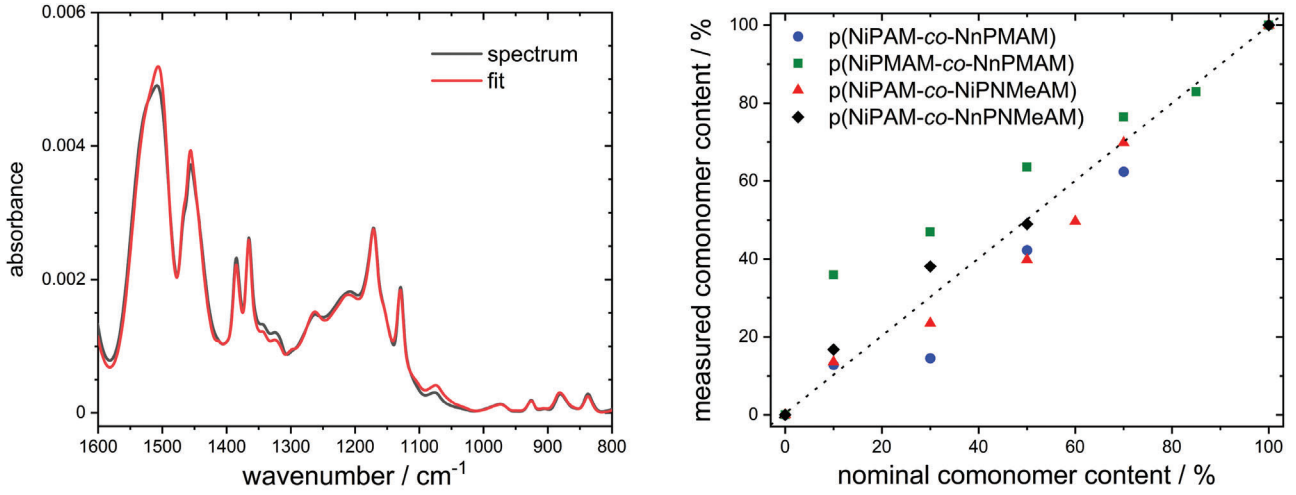

Figure 5. Determination of the copolymer microgel composition by ATR-FTIR spectroscopy. a) Example of an FTIR spectrum fitted by a linear combination of the reference spectra. b) Copolymerization ratio calculated from the ATR-FTIR spectra. The dashed line represents the equivalence between nominal monomer feed and measured real incorporated comonomer content.

of NnPMAM is favored and the monomer is incorporated with a higher efficiency than expected (Figure 5b green ▼). This means more NiPMAM stays in solution in form of un-reacted monomer or in form of oligomers which did not precipitate on the formed particles. This difference between the two copolymer systems is probably caused by a different particle formation mechanism and kinetics of the first monomer NiPAM or NiPMAM during the polymerization process. Similar behavior has also been observed earlier.[50]

2.3.2. PCS of Copolymer Microgels

Angle dependent PCS measurements are done and the obtained correlation functions are evaluated by inverse Laplace transformation (CONTIN)[63,64] and with the method of cumulants.[65,66] Both methods yield the same results. A linear dependency of the mean relaxation rate on q^2 was obtained for all copolymers at 10 and 55 °C. From a linear fit of the data the translational diffusion coefficient D^T is obtained and the hydrodynamic radius can be calculated. For more clarity only the values of the hydrodynamic radius obtained from the CONTIN analysis are shown.

In **Figure 6** the hydrodynamic radius for all synthesized copolymer microgels at 10 and 55 °C as a function of the comonomer content is summarized. To achieve good comparability of the data with each other, the scale of the radius axis was chosen to be equal in all shown plots.

The first obvious difference between the dimensions of all copolymers is that the microgel particles with NiPMAM as first monomer are in general larger than the particles with NiPAM (see Figure 6a,b). This is comparable to our previous results.[50,67]

The hydrodynamic radius of the copolymer system consisting of P(NiPAM-*co*-NnPMAM) (Figure 6a) increases at 10 and 55 °C slightly with increasing content of the new monomer and reaches the highest value for pure PNnPMAM. In contrast to this, the overall microgel size of P(NiPMAM-*co*-NnPMAM) shows the opposite trend, it is nearly constant at low comonomer contents and subsequently decreases at higher NnPMAM contents (Figure 6b).

For the copolymer system P(NiPAM-*co*-NiPNMeAM) no systematic change in R_h is visible and therefore an additional methyl group present at the nitrogen atom of NiPAM does not influence the microgel dimensions. This is in contrast to the system based on P(NiPAM-*co*-NnPNMeAM). Here, R_h increases with the amount of the second monomer NnPNMeAM. Accordingly, the sizes of swollen and collapsed microgels can be precisely tuned by admixture of methylated comonomers in the synthesis.

2.3.3. AFM of the Copolymer Microgels

To investigate the influence of the alternative monomers on the structure of copolymer microgels with NiPAM (or NiPMAM) the particles are characterized by AFM in addition. Representative for all copolymer microgels, the AFM pictures of the 50/50 mixtures of the four different systems are shown in **Figure 7** and the corresponding height images are given in the Supporting Information (Figure S2). At a first glance, it can be clearly seen that the copolymer particles show a circular lateral cross section in all cases.

The microgels based on NiPMAM in combination with NnPMAM (see Figure 7b) show a tendency to aggregate during the drying process in the AFM sample preparation procedure. This aggregation maybe caused by different interactions (interparticle and with the surface of the inorganic substrate) when NiPMAM is used as first monomer instead of NiPAM. The microgels in Figure 7a,b appear as homogeneous particles with no recognizable core–shell structure. Therefore a statistical distribution of the monomer components in the microgel network is assumed.

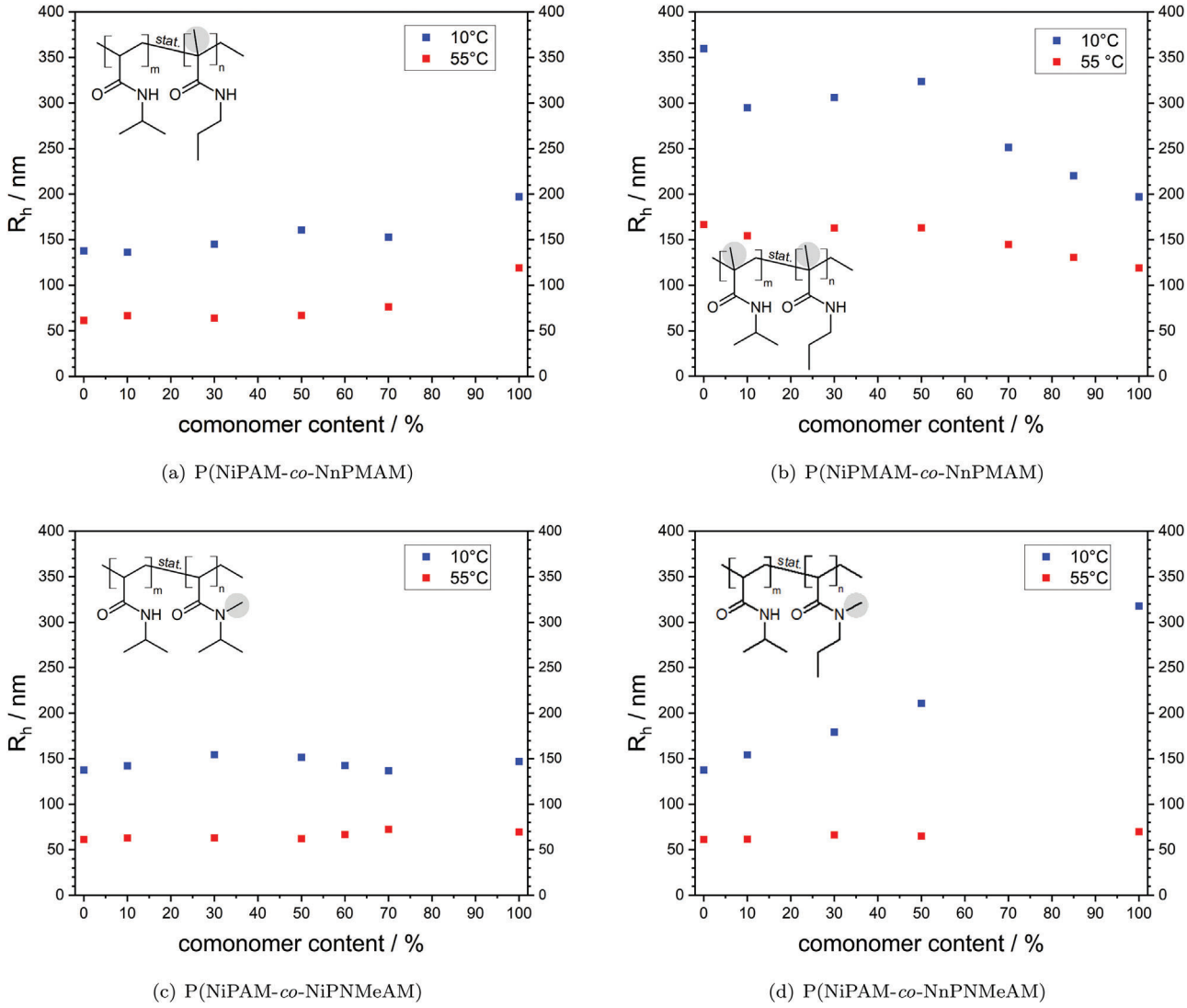

Figure 6. Hydrodynamic radius at 10 and 55 °C as a function of the comonomer content for different copolymer microgels: a) P(NiPAM-*co*-NnPMAM), b) P(NiPMAM-*co*-NnPMAM), c) P(NiPAM-*co*-NiPNMeAM), and c) P(NiPAM-*co*-NnPNMeAM).

A closer view on the AFM images in Figure 7c,d indicates, similar to the homopolymers, that the copolymer systems with NnPNMeAM and NiPNMeAM also appear significantly flatter in the adsorbed state than the microgels with NnPMAM. Here, for the 50/50 mixture of NiPNMeAM with NiPAM also homogenous particles are visible suggesting statistical copolymerization. Only the images of the 50/50 mixture of NnPNMeAM with NiPAM suggest a slight core–shell structure. This could be caused by unequal incorporation of the two monomers into the microgel network, but also an altered interaction with the crosslinker BIS could lead to the formation of a particle with core–shell structure.

2.4. Swelling Behavior of the Copolymer Microgels

The swelling behavior in aqueous solution was first investigated using temperature dependent PCS measurements which monitor the decrease in hydrodynamic radius of the microgel particles when the temperature is increased. The obtained curves for all copolymer microgels are summarized in **Figures 8** and **9**. Furthermore, the first derivative of the swelling curves was numerically calculated to identify the VPTT of the microgels.

The copolymer microgels P(NiPAM-*co*-NnPMAM) and P(NiMPAM-*co*-NnPMAM) show a linear dependence between the comonomer content and the value of the transition temperature. This leads to the assumption that during the formation process of the polymer the two monomers are randomly incorporated in the microgel network and a statistical copolymer is formed. This observation also supports the results from the AFM images.

The combination of NiPAM and NiPNMeAM yields particles that show a linear dependence of the VPTT on the comonomer content up to 70% NiPNMeAM. From this content on, the VPTT does not seem to change anymore and approximately has the same value of 19 °C as that of NiPNMeAM homopolymer microgel.

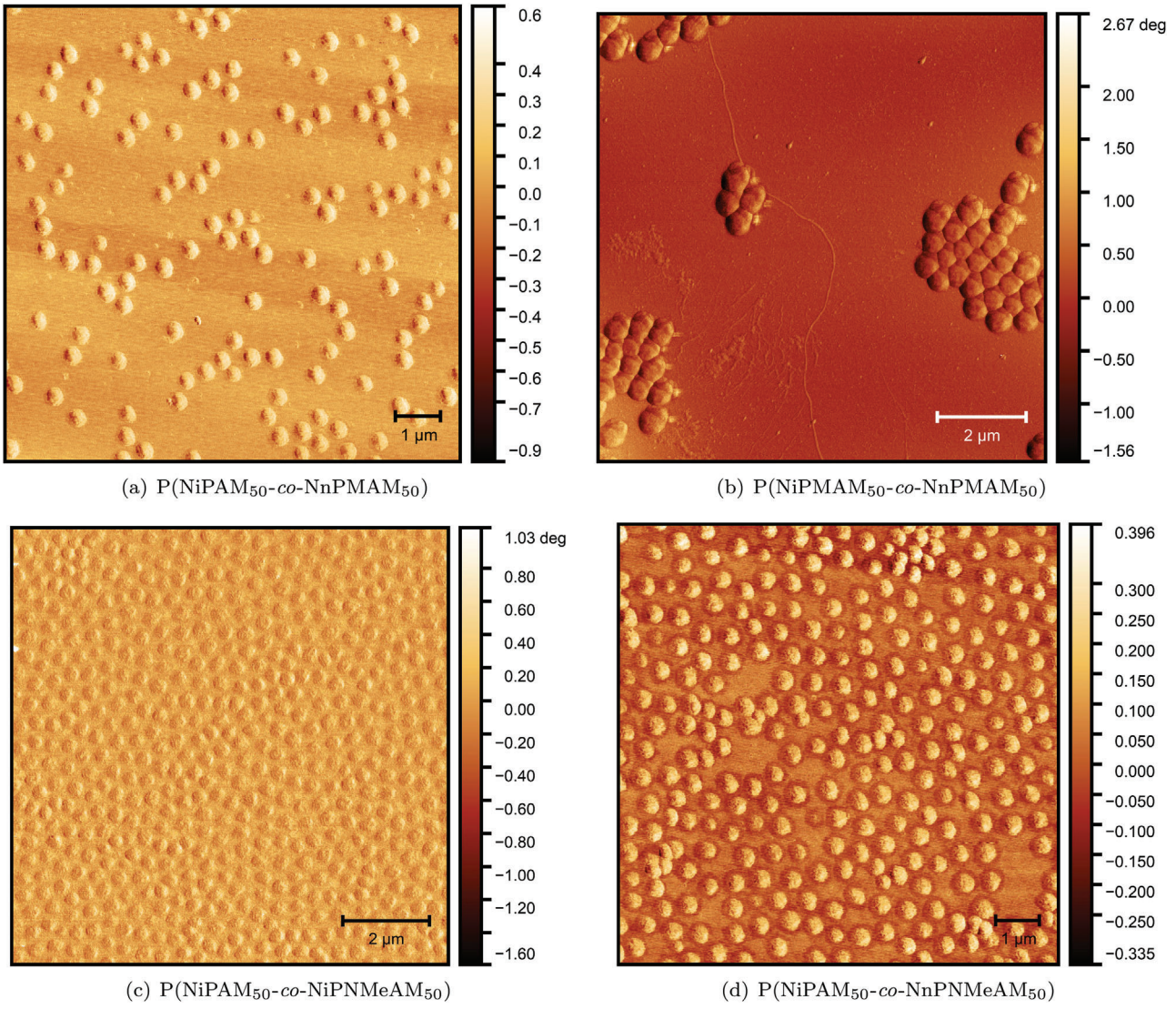

Figure 7. AFM phase images of the copolymer microgels at a comonomer content of 50% a) P(NiPAM-*co* -NnPMAM), b) P(NiPMAM-*co*-NnPMAM), c) P(NiPAM-*co*-NiPNMeAM), and d) P(NiPAM-*co*-NnPNMeAM).

P(NiPAM-*co*-NnPNMeAM) exhibits a similar but more pronounced behavior. The VPTT is approximately constant from a comonomer content of 50% on and therefore additional synthesis are necessary in the future to clarify the trend of the VPTT observed with PCS. We find that admixtures of all methylated comonomers besides NnPNMeAm lead to a strong change in VPTT of up to 16 K, whereas the observed change with NnPNMeAm is only 7 K.

2.4.1. Temperature-Dependent FTIR Measurements

To gain additional information about the particle morphology and to support the results from the temperature dependent PCS measurements concerning the phase transition, FTIR spectroscopy was used to follow the temperature induced shift of the maximum of the NH-band.[68] In **Figure 10** the spectral position of the NH-band maximum is plotted against the temperature for two copolymer systems (P(NiPAM-*co*-NnPMAM) and P(NiMPAM-*co*-NnPMAM)). First, at temperatures where no phase transition occurs, a small and steady shift can be observed, which is attributed to a temperature-dependent change in water structure.[68,69] In the phase transition temperature region the hydrogen bonding between the polymer chains and the solvent changes significantly and therefore an obvious shift of the NH-band is recognizable. The temperature-dependent data, obtained in this way, is then fitted to describe temperature and broadness of the phase transition quantitatively. It was possible to apply only one error function to fit the measured data indicating that the two combined monomers form a statistical copolymer. If the particles would exhibit a more complex architecture resembling for example a core–shell like composition gradient[68] or larger homopolymer domains,[70] two error functions would be required for fitting.

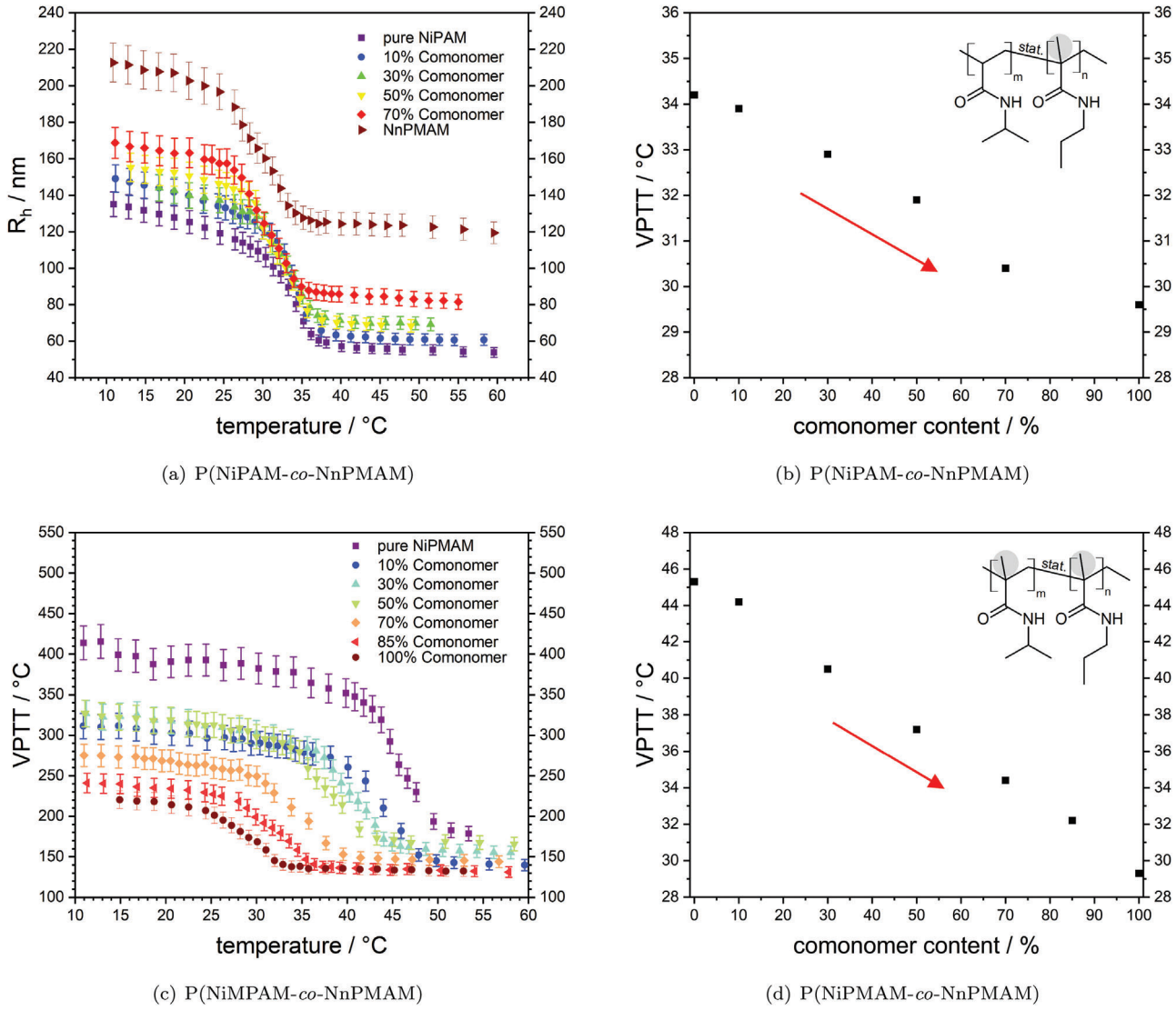

(a) P(NiPAM-*co*-NnPMAM)

(b) P(NiPAM-*co*-NnPMAM)

(c) P(NiMPAM-*co*-NnPMAM)

(d) P(NiPMAM-*co*-NnPMAM)

Figure 8. Temperature dependent swelling curves of the copolymer microgels based on NiPAM/NiPMAM a/c) in combination with NnPMAM. For the determination of the VPTT the first derivative of the swelling curves and its point of inflection is used. The calculated VPTTs are summarized in the graphs (b) and (d). The red arrows are guides to the eye.

In the case of the copolymer microgel P(NiPAM-*co*-NiPNMeAM) the C=O band was analyzed due to the lack of a NH-vibration in the NiPNMeAM monomer. Here it should be mentioned that the shift of the C=O stretching vibration shows the opposite trend compared to the NH bending vibration. Additionally, D_2O was used as solvent instead of H_2O because the characteristic H_2O band superimposes the contribution by the C=O vibration. The obtained results are represented in **Figure 11**a. For fitting only one error function was used indicating the formation of statistical copolymer microgels. From the swelling curves the VPTTs were determined as summarized in Figure 11b including the results from P(NiPAM-*co*-NnPMAM) and P(NiMPAM-*co*-NnPMAM).

A comparison with the VPTT values from the temperature-dependent PCS measurements of the NnPMAM copolymer microgels (Figure 8) shows a similar dependency of the VPTT on the comonomer content in the microgel particles (see **Table 2**). The copolymer microgels with NnPMAM as second monomer follow the expected trend of a linear relation between monomer composition and VPTT, which supports the assumption of a statistical copolymer formation.[38]

However, if a methyl group at the nitrogen atom of the acrylamide monomer is present (here in the case of NiPNMeAM) it seems to have drastic influence on the phase transition, causing a deviation from the expected linear relationship. At higher comonomer contents (>40 mol%) the VPTT stays nearly constant at a value comparable to the VPTT of the NiPNMeAM homopolymer (≈23.6 °C). This behavior was also observed in the PCS data, however, less pronounced. Here, the VPTT only remains constant at comonomer contents higher than 70 mol%. This difference may be caused by the fact that D_2O was used as solvent instead of H_2O for the IR measurements. This would also

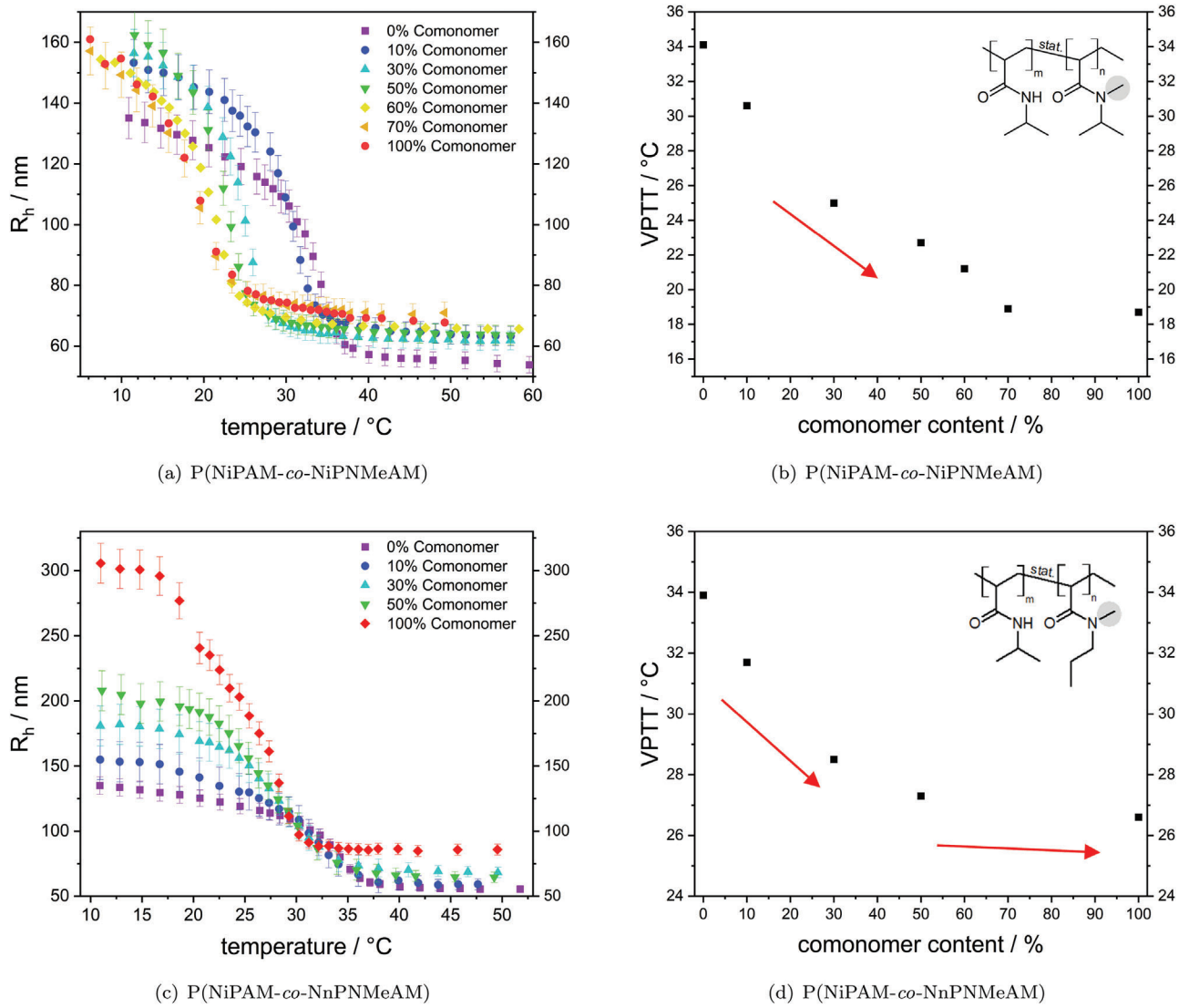

(a) P(NiPAM-*co*-NiPNMeAM)

(b) P(NiPAM-*co*-NiPNMeAM)

(c) P(NiPAM-*co*-NnPNMeAM)

(d) P(NiPAM-*co*-NnPNMeAM)

Figure 9. Temperature dependent swelling curves of the copolymer microgels a) NiPAM/NiPNMeAM and c) NiPAM/NnPNMeAM. For the determination of the VPTT the first derivative of the swelling curves is used to determine the point of inflection. The calculated VPTTs are summarized in the graphs (b) and (d). The red arrows are guides to the eye.

explain the difference in the IR- and PCS-VPTT of the NiPNMeAM homopolymer. Therefore, the NiPNMeAM homopolymer microgel was additionally characterized in D_2O using temperature-dependent PCS. According to FTIR spectroscopy, the phase transition of the homopolymer is strongly broadened by N-methylation and the collapse occurs at a 3 K higher temperature than determined by PCS. This unusual deviation might be explained by the special monomer structure, which does not allow any direct hydrogen bonding interaction between the monomers. Accordingly, (heavy) water molecules are strongly bound in between the monomers and released at higher temperatures than the collapse of the global structure of the particle. This observation might be referred to as a delayed-release behavior and requires further investigation. Accordingly, in this case the VPTT is not clearly defined but strongly depends on the observed quantity.

The effect of a non-linear dependence of the comonomer content and the VPTT might hint toward a favorable self-interaction of NiPnMeAM during polymerization. However, this contradicts the fact that the amount of incorporated comonomer corresponds to the used monomer feed (see Figure 5, black diamonds). At present we do not have a full explanation for this behavior.

3. Conclusion

The present article reports the synthesis of smart microgels based in alternative acrylamides which were partially not yet used for this purpose. All monomers were found to form microgel particles with low polydispersities in the classical precipitation polymerization approach. The found VPTTs range from 18.7 to 45.3 °C. By copolymerization of the alternative monomers with "classical" NiPAM, NiPMAM, and NnPAM, microgels were ob-

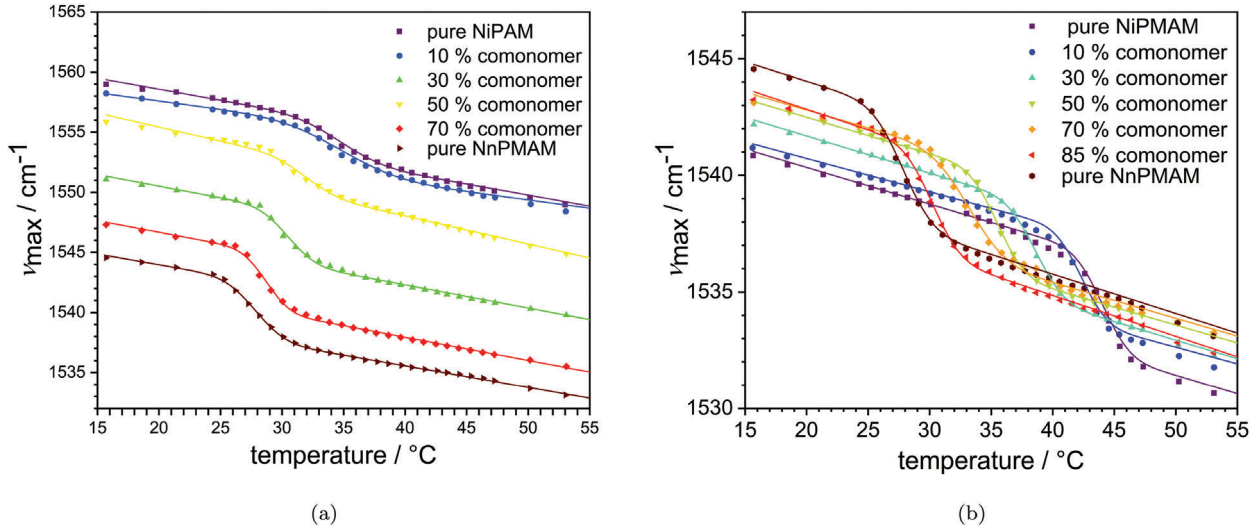

Figure 10. Swelling behavior of copolymer microgels from a) P(NiPAM-*co*-NnPMAM) and b) P(NiMPAM-*co*-NnPMAM) investigated by temperature dependent FTIR spectroscopy of the NH-bending vibration in H_2O. ν_{max} is the maximum position of the analyzed band. The lines indicate fits with a sum of a second degree polynomial and an error function.

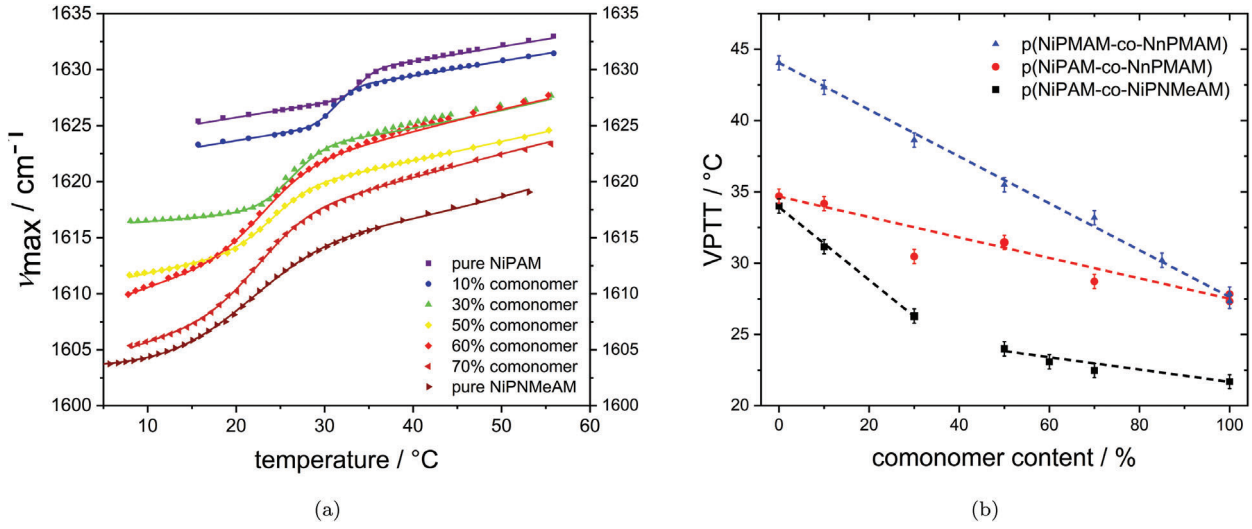

Figure 11. a) Swelling behavior of copolymer microgels from P(NiPAM-*co*-NiPNMeAM) investigated by temperature dependent FTIR spectroscopy of the C=O-stretching vibration in D_2O. The lines indicate fits with a sum of a second degree polynomial and an error function. b) Plot of the VPTT versus the comonomer content for three copolymer systems.

Table 2. VPTTs of the homopolymers obtained from the PCS swelling curves and from the temperature-dependent FT-IR measurements.

	NiPAM	NiPMAM	NiPNMeAM	NnPAM	NnPMAM	NnPNMeAM
$VPTT_{PCS}$	34.2 °C	45.3 °C	18.7 °C	22.8 °C	29.6 °C	26.6 °C
$VPTT_{FTIR}$	34.7 °C	44.0 °C	21.7 °C	24.6 °C[a)]	27.8 °C	/ °C

[a)] From ref. [68]; Was measured for particles which were made by a different synthesis procedure.

tained which exhibit varying transition temperatures between the two limiting values mentioned above. Also for the copolymer microgels a low polydispersity was shown using AFM. The copolymer content was quantified by using FTIR spectroscopy. An expected copolymerization behavior was found for copolymer microgels from NiPNMeAM and NnPNMeAM, while slight deviations were found for the monomer NNPMAM. The swelling behavior was studied using temperature dependent PCS and FTIR indicating the successful formation of statistical copolymer microgels. Regarding phase transitions, an interesting behavior was found for the monomers NiPNMeAM and NnPNMeAM, that will be further elucidated in future work.

The present work provides a complete library of copolymer microgels having tunable transition temperatures. This allows to adapt the particles for the desired temperature range of an application. Moreover, the swelling curves of these microgels might provide a good data base for testing the Flory–Rehner description of swelling of statistical copolymer micro gelsystems.

4. Experimental Section

Materials: For the synthesis of the alternative acrylamides acryloyl chloride (97%, 200 ppm 4-methoxyphenol, Sigma-Aldrich Chemie GmbH, Taufkirchen, Germany), *N*-isopropylmethylamine (98%, Sigma-Aldrich Chemie GmbH, Taufkirchen, Germany), *n*-propylamine (98%, (Acros organics, Fischer Scientific GmbH, Schwerte, Germany), triethylamine (Janssen-Cilag GmbH, Neuss, Germany, 99%), *N*-methylpropylamine (96%, Acros organics, Fischer Scientific GmbH, Schwerte, Germany) were used as received. Methacryloyl chloride (97%, 200 ppm monomethyl ether hydroquinone, Sigma-Aldrich Chemie GmbH, Taufkirchen, Germany) was purified by vacuum destillation.

Additionally*N*-isoproplyacrylamide (NiPAM) (97%, Sigma-Aldrich Chemie GmbH, Taufkirchen, Germany; recrystallized from *n*-hexane), *N,N*-methylenebisacrylamide (BIS), *N*-isopropylmethacrylamide (NiPMAM) (97%, Sigma-Aldrich Chemie GmbH, Taufkirchen, Germany; recrystallized from *n*-hexane), sodium dodecyl sulfate (SDS) (≥ 99%, Sigma-Aldrich Chemie GmbH, Taufkirchen, Germany), and ammonium persulfate (APS) (≥ 98%, Sigma-Aldrich Chemie GmbH, Taufkirchen, Germany) were used for the microgel synthesis. Water was purified using an Arium pro VF system (Sartorius Stedim, Göttingen, Germany). All other reagents and solvents were used as received.

Monomer Synthesis: For the monomer synthesis acryloyl chloride or methacryloyl chroride in dichloromethane was slowly added under continuous stirring to the corresponding alkylamine in dichloromethane at 0°C. The mixture was warmed up to room temperature (RT) and the reaction was continued for 12 h. Afterward the solution was purified by filtration, extraction, and destillation. For a detailed description of the synthesis procedure see Supporting Information.

Microgel Synthesis: For the preparation of the alternative homo- and copolymer microgels, first a synthesis procedure to perform a precipitation polymerization was developed. This procedure represented a downscaled version of the original synthesis introduced by Chibante and Pelton.[1] Therefore, a setup with a 25 mL two-neck flask equipped with a reflux condenser, magnetic stirrer (600 rpm) and a nitrogen inlet was used. The monomers (total concentration 77 mmol L^{-1}) and the cross-linker BIS (4.12 mmol $L^{-1} \approx 5.35$ mol% with respect to the total monomer amount) were dissolved in 10 mL purified water and were heated up to 80 °C oil bath temperature under continuous stirring and purged with nitrogen. After 50 min the surfactant (1.1 mmol L^{-1}) was added and the system was equilibrated for another 10 min. The polymerization was initiated by the addition of 38 µL of a 0.71 mol L^{-1} APS solution and left to proceed for 4 h at 80 °C. After this reaction time the microgel solution was cooled to room temperature and stirred overnight. For purification all samples had been treated at least three times by centrifugation, decantation, and redispersion using purified water.

NMR: The ^{1}H-NMR spectra were recorded on a Bruker DRX 500 spectrometer (Bruker, Rheinstetten, Germany) in $CDCl_3$ at 298 K. As reference the proton signal of residual chloroform ($\delta = 7.26$ ppm) was used. The fine structure of the signals is described by s=singlet, d=doublet, t=triplet, m=multiplet, and br=broad signal. The detailed analysis of the spectra is summarized in the Supporting Information.

Photon Correlation Spectroscopy: For the light scattering experiments microgel concentrations below 0.001wt% and different optical setups were used. The angle dependent measurements were performed using a goniometer set-up (ALV Langen, Germany) equipped with a multiple-τ digital correlator ALV-5000/E (ALV-GmbH, Langen, Germany). The used light source was an argon-ion laser (Spectra Physics Stabilite 2017, Newport Corporation, USA; $\lambda = 514.5$ nm) and alternately with a 3D-LS Spectrometer (LS Instruments AG, Fribourg, Switzerland) equipped with a HeNe laser (JDSU 1145P, Thorlabs Inc., Newton, NJ, USA; $\lambda = 632.8$ nm). Furthermore, the temperature dependent measurements were done at a constant scattering angle of 60° using a custom built setup equipped with a solid-state laser at $\lambda = 661.4$ nm (TOPTICA Photonics AG, Germany) or with a HeNe laser (HNL210L, Thorlabs Inc., USA; $\lambda = 632.8$ nm). To generate the time-intensity autocorrelation function an ALV-6010 multiple-τ correlator (ALV-GmbH, Langen, Germany) was used in this machine.

In all three employed setups the sample temperature was adjusted using a temperature controlled decaline bath and all measurements were repeated at least three times. The measured autocorrelation functions were analyzed by inverse Laplace transformation[63,64] and in addition by the method of cumulants.[65,66] The obtained values for the relaxation rate Γ were subsequently averaged on basis of the three individual measurements. The obtained mean relaxation rate $\overline{\Gamma}$ was used to calculate the translational diffusion coefficient D^T for diluted particle solution via $\overline{\Gamma} = D^T \cdot q^2$ (with q being the magnitude of the scattering vector defined by $q = \frac{4\pi n}{\lambda} \sin \frac{\theta}{2}$; with λ being the used wavelength of the laser and n the refractive index of the sample). Furthermore, using the Stokes–Einstein equation a calculation of the mean apparent hydrodynamic radius R_h of the microgel particles is possible.

Atomic Force Microscopy: The measurements were performed with a DI Nanoscope IIIa (Digital Instruments, now Bruker, Karlsruhe, Germany) mounted on a Zeiss Axiovert 135 inverted microscope (Carl Zeiss Microscopy GmbH, Jena, Germany) in semi-contact mode using Budget Sensors (Innovative Solution Bulgaria Ltd., Sofia, Bulgaria) Al-Reflex Tap300Al-G cantilevers with a tip radius of < 10 nm, a resonance frequency of about 300 kHz and a spring constant of 40 N m^{-1}.

For the sample preparation the silicon wafers (Siegert Wafer GmbH, Aachen, Germany) were cleaned with ethanol (HPLC grade) in a plasma cleaner (Zepto, Diener Electronics, Ebhausen, Germany). Afterward the wafers were successively spin-coated with a PEI-solution (0.1 mL; 0.25 wt%) and a highly-diluted microgel suspension ($c \leq 0.01$ wt%) at 1000 rpm.

FT-IR Spectroscopy: To quantify the amount of the different monomers present in the copolymer microgels, ATR-FTIR spectroscopy was performed on a FT-IR spectrometer (IFS66/s, Bruker, Ettlingen, Germany), equipped with a diamond single reflection ATR cell (Golden Gate, Specac, Kent, UK) and a mercury cadmium telluride detector. 15 µL of the microgel suspensions were dropped onto the crystal and dried in a stream of dry air for about 10 min until a steady FTIR spectrum was detected. The FTIR spectra were acquired with a resolution of 2 cm^{-1} with air as reference. Three different films of each sample were measured and averaged to obtain the final spectrum.

In GNU Octave[71] the spectra were normalized to the integral and fitted with a linear combination of the spectra of the respective homopolymer microgels in the spectral region from 1600 to 800 cm^{-1}. From the coefficients of the linear combination the degree of copolymerization was calculated.

For the temperature-dependent measurements a Tensor 27 FTIR spectrometer (Bruker, Ettlingen, Germany) in transmission mode with cuvettes specially made from BaF_2 (Korth Kristalle, Kiel, Germany) was used. At each temperature the absorbance spectra were calculated from the copolymer microgel spectrum and as reference the spectrum of H_2O whereby the water absorbance was corrected for algorithmically as described before.[70] Afterward, the maximal frequencies of the temperature-dependent NH– or C=O–bands were extracted and plotted versus the temperature. To quantify the phase transition the data were fitted with a sum of a second degree polynomial and an error function according to previous work.[68]

Supporting Information

Supporting Information is available from the Wiley Online Library or from the author.

Acknowledgements

The authors thank Jörn Lessmeier and Johanna Grote for their help in the monomer synthesis.

Open access funding enabled and organized by Projekt DEAL.

Conflict of Interest

The authors declare no conflict of interest.

Data Availability Statement

Research data are not shared.

Keywords

acrylamide, atomic force microscopy, nanogels, photon correlation spectroscopy, precipitation polymerization

Received: February 23, 2021
Revised: May 6, 2021
Published online:

[1] R. H. Pelton, P. Chibante, *Colloids Surf.* **1986**, *20*, 247.
[2] M. Murray, M. Snowden, *Adv. Colloid Interf. Sci.* **1995**, *54*, 73.
[3] R. Pelton, *Adv. Colloid Interf. Sci.* **2000**, *85*, 1.
[4] S. Nayak, L. A. Lyon, *Angew. Chem. Int. Ed.* **2005**, *44*, 7686.
[5] A. Z. Pich, H.-J. P. Adler, *Polym. Int.* **2007**, *56*, 291.
[6] W. Richtering, A. Pich, *Soft Matter* **2012**, *8*, 11423.
[7] Y. Hertle, T. Hellweg, *J. Mater. Chem. B* **2013**, *43*, 5874.
[8] W. Richtering, B. R. Saunders, *Soft Matter* **2014**, *10*, 3695.
[9] S. Wellert, M. Richter, T. Hellweg, R. von Klitzing, Y. Hertle, *Z. Phys. Chem.* **2015**, *229*, 1225.
[10] F. A. Plamper, W. Richtering, *Acc. Chem. Res.* **2017**, *50*, 131.
[11] M. Karg, A. Pich, T. Hellweg, T. Hoare, L. A. Lyon, J. J. Crassous, D. Suzuki, R. A. Gumerov, S. Schneider, I. I. Potemkin, W. Richtering, *Langmuir* **2019**, *35*, 6231.
[12] G. M. Conley, S. Nojd, M. Braibanti, P. Schurtenberger, F. Scheffold, *Colloids Surf., A* **2016**, *499*, 18.
[13] J. J. Crassous, M. Siebenbürger, M. Ballauff, M. Drechsler, O. Henrich, M. Fuchs, *J. Chem. Phys.* **2006**, *125*, 204906.
[14] M. F. Schulte, A. Scotti, M. Brugnoni, S. Bochenek, A. Mourran, W. Richtering, *Langmuir* **2019**, *35*, 14769.
[15] J. Gao, B. J. Frisken, *Langmuir* **2003**, *19*, 5212.
[16] J. Dubbert, K. Nothdurft, M. Karg, W. Richtering, *Macromol. Rapid Commun.* **2014**, *36*, 159.
[17] J. Dubbert, T. Honold, J. S. Pedersen, A. Radulescu, M. Drechsler, M. Karg, W. Richtering, *Macromolecules* **2014**, *47*, 8700.
[18] M. Karg, S. Wellert, S. Prevost, R. Schweins, C. Dewhurst, L. M. Liz-Marzán, T. Hellweg, *Coll. Polym. Sci.* **2011**, *289*, 699.
[19] A. Scotti, J. E. Houston, M. Brugnoni, M. M. Schmidt, M. F. Schulte, S. Bochenek, R. Schweins, A. Feoktystov, A. Radulescu, W. Richtering, *Phys. Rev. E* **2020**, *102*, 5.
[20] M. F. Schulte, S. Bochenek, M. Brugnoni, A. Scotti, A. Mourran, W. Richtering, *Angew. Chem., Int. Ed.* **2020**, *60*, 2280.
[21] K. Uhlig, T. Wegener, J. He, M. Zeiser, J. Bookhold, I. Dewald, N. Godino, M. Jaeger, T. Hellweg, A. Fery, C. Duschl, *Biomacromolecules* **2016**, *17*, 1110.
[22] K. Uhlig, T. Wegener, Y. Hertle, J. Bookhold, M. Jaeger, T. Hellweg, A. Fery, C. Duschl, *Polymers* **2018**, *10*, 656.
[23] Q. M. Zhang, D. Berg, S. M. Mugo, M. J. Serpe, *Chem. Commun.* **2015**, *51*, 9726.
[24] Q. M. Zhang, D. Berg, J. Duan, S. M. Mugo, M. J. Serpe, *ACS Appl. Mater. Interfaces* **2016**, *8*, 27264.
[25] C. M. Nolan, M. J. Serpe, L. A. Lyon, *Biomacromolecules* **2004**, *5*, 1940.
[26] S. Berger, H. Zhang, A. Pich, *Adv. Func. Mater.* **2009**, *19*, 554.
[27] L. Zha, B. Banik, F. Alexis, *Soft Matter* **2011**, *7*, 5908.
[28] D. V. Pergushov, L. V. Sigolaeva, N. G. Balabushevich, T. Z. Sharifullin, M. Noyong, W. Richtering, *Polymer* **2021**, *213*, 123227.
[29] M. Das, N. Sanson, D. Fava, E. Kumacheva, *Langmuir* **2007**, *23*, 196.
[30] Y. Lu, Y. Mei, M. Ballauff, M. Drechsler, *J. Phys. Chem. B* **2006**, *110*, 3930.
[31] T. Brändel, V. Sabadasch, Y. Hannappel, T. Hellweg, *ACS Omega* **2019**, *4*, 4636.
[32] V. Boyko, S. Richter, A. Pich, K.-F. Arndt, *Colloid Polym. Sci.* **2003**, *282*, 127.
[33] A. Balaceanu, V. Mayorga, W. Lin, M.-P. Schürings, D. E. Demco, A. Böker, M. A. Winnik, A. Pich, *Colloid Polym. Sci.* **2012**, *291*, 21.
[34] I. Berndt, J. S. Pedersen, P. Lindner, W. Richtering, *Langmuir* **2006**, *22*, 459.
[35] K. von Nessen, M. Karg, T. Hellweg, *Polymer* **2013**, *54*, 5499.
[36] O. Wrede, Y. Reimann, S. Lülsdorf, D. Emmrich, K. Schneider, A. J. Schmid, D. Zauser, Y. Hannappel, A. Beyer, R. Schweins, A. Gölzhäuser, T. Hellweg, T. Sottmann, *Sci. Rep.* **2018**, *8*, 13781.
[37] O. Wrede, S. Bergmann, Y. Hannappel, T. Hellweg, T. Huser, *Soft Matter* **2020**, *16*, 8078.
[38] B. Wedel, M. Zeiser, T. Hellweg, *Z. Phys. Chem* **2012**, *226*, 737.
[39] J.-H. Kim, M. Ballauff, *Colloid Polym. Sci.* **1999**, *277*, 1210.
[40] T. Hoare, R. Pelton, *Langmuir* **2004**, *20*, 2123.
[41] B. R. Saunders, H. M. Crowther, B. Vincent, *Macromolecules* **1997**, *30*, 482.
[42] S. Zhou, B. Chu, *J. Phys. Chem. B* **1998**, *102*, 1364.
[43] M. Martinez-Moro, J. Jenczyk, J. M. Giussi, S. Jurga, S. E. Moya, *J. Colloid Interface Sci.* **2020**, *580*, 439.
[44] T. Hoare, R. Pelton, *Langmuir* **2006**, *22*, 7342.
[45] T. Hirano, K. Nakamura, T. Kamikubo, S. Ishii, K. Tani, T. Mori, T. Sato, *J. Polym. Sci., Part A: Polym. Chem.* **2008**, *46*, 4575.
[46] G. Yuan, X. Yin, L. Sun, M. Cui, Z. Yuan, C. Wang, M. Yin, L. Wang, *ACS Appl. Mater. Interfaces* **2012**, *4*, 950.
[47] V. Chytrý, M. Netopilík, M. Bohdanecký, K. Ulbrich, *J. Biomater. Sci., Polym. Ed.* **1997**, *8*, 917.
[48] Y. Maeda, T. Nakamura, I. Ikeda, *Macomolecules* **2001**, *34*, 1391.
[49] M. Kano, E. Kokufuta, *Langmuir* **2009**, *25*, 8649.
[50] B. Wedel, Y. Hertle, O. Wrede, J. Bookhold, T. Hellweg, *Polymers* **2016**, *8*, 162.
[51] S. Ito, *Kobunshi Ronbunshu* **1989**, *46*, 437.
[52] Y. Maeda, T. Nakamura, I. Ikeda, *Macromolecules* **2001**, *34*, 8246.
[53] A. Elaissari, *Colloidal Polymers - Synthesis and Characterization*, 1st ed., Marcel Dekker, Inc., New York, NY **2003**.
[54] Y. Matsumura, K. Iwai, *Polymer* **2005**, *46*, 10027.
[55] S. Uchiyama, Y. Matsumura, A. P. de Silva, K. Iwai, *Anal. Chem.* **2004**, *76*, 1793.
[56] M. Zeiser, I. Freudensprung, T. Hellweg, *Polymer* **2012**, *53*, 6096.
[57] V. Sabadasch, L. Wiehemeier, T. Kottke, T. Hellweg, *Soft Matter* **2020**, *16*, 5422.
[58] J. Oberdisse, T. Hellweg, *Colloid Polym. Sci.* **2020**, *298*, 921.
[59] M. Cors, L. Wiehemeier, O. Wrede, A. Feoktystov, F. Cousin, T. Hellweg, J. Oberdisse, *Soft Matter* **2020**, *16*, 1922.
[60] P. Otto, S. Bergmann, A. Sandmeyer, M. Dirksen, O. Wrede, T. Hellweg, T. Huser, *Nanoscale Adv.* **2020**, *2*, 323.
[61] S. Fujishige, K. Kubota, I. Ando, *J. Phys. Chem.* **1989**, *93*, 3312.
[62] D. Duracher, A. Elaïssari, C. Pichot, *Colloid Polym. Sci.* **1999**, *277*, 905.
[63] S. W. Provencher, *Comput. Phys. Commun.* **1982**, *27*, 213.
[64] S. W. Provencher, *Comput. Phys. Commun.* **1982**, *27*, 229.
[65] D. E. Koppel, *J. Chem. Phys.* **1972**, *57*, 4814.
[66] P. Hassan, S. Kulshreshtha, *J. Polym. Interface Sci.* **2006**, *300*, 744.
[67] B. Wedel, T. Brändel, J. Bookhold, T. Hellweg, *ACS Omega* **2017**, *2*, 84.
[68] L. Wiehemeier, M. Cors, O. Wrede, J. Oberdisse, T. Hellweg, T. Kottke, *Phys. Chem. Chem. Phys.* **2019**, *21*, 572.
[69] F. O. Libnau, J. Toft, A. A. Christy, O. M. Kvalheim, *J. Am. Chem. Soc.* **1994**, *116*, 8311.
[70] L. Wiehemeier, T. Brändel, Y. Hannappel, T. Kottke, T. Hellweg, *Soft Matter* **2019**, *15*, 5673.
[71] J. W. Eaton, D. Bateman, S. Hauberg, R. Wehbring, *GNU Octave Version 4.2.0 Manual: A high-level interactive language for numerical computations*, Free Software Foundation, Boston, MA **2016**.

